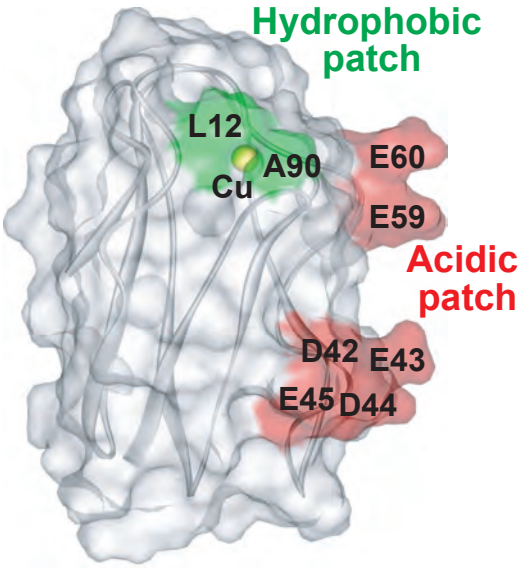

Supplementary Fig. 1 Distribution of the hydrophobic and acidic patches in spinach Pc.
The surface of Pc is transparent, and the copper atom and the ribbon diagram are simultaneously displayed. The residues in the hydrophobic and acidic patches that were proposed to be responsible for the electron transport in previous mutational analyses are labeled, and colored green and red, respectively. The molecular diagrams were generated with Web Lab Viewer Pro (Molecular Simulations, Inc.).

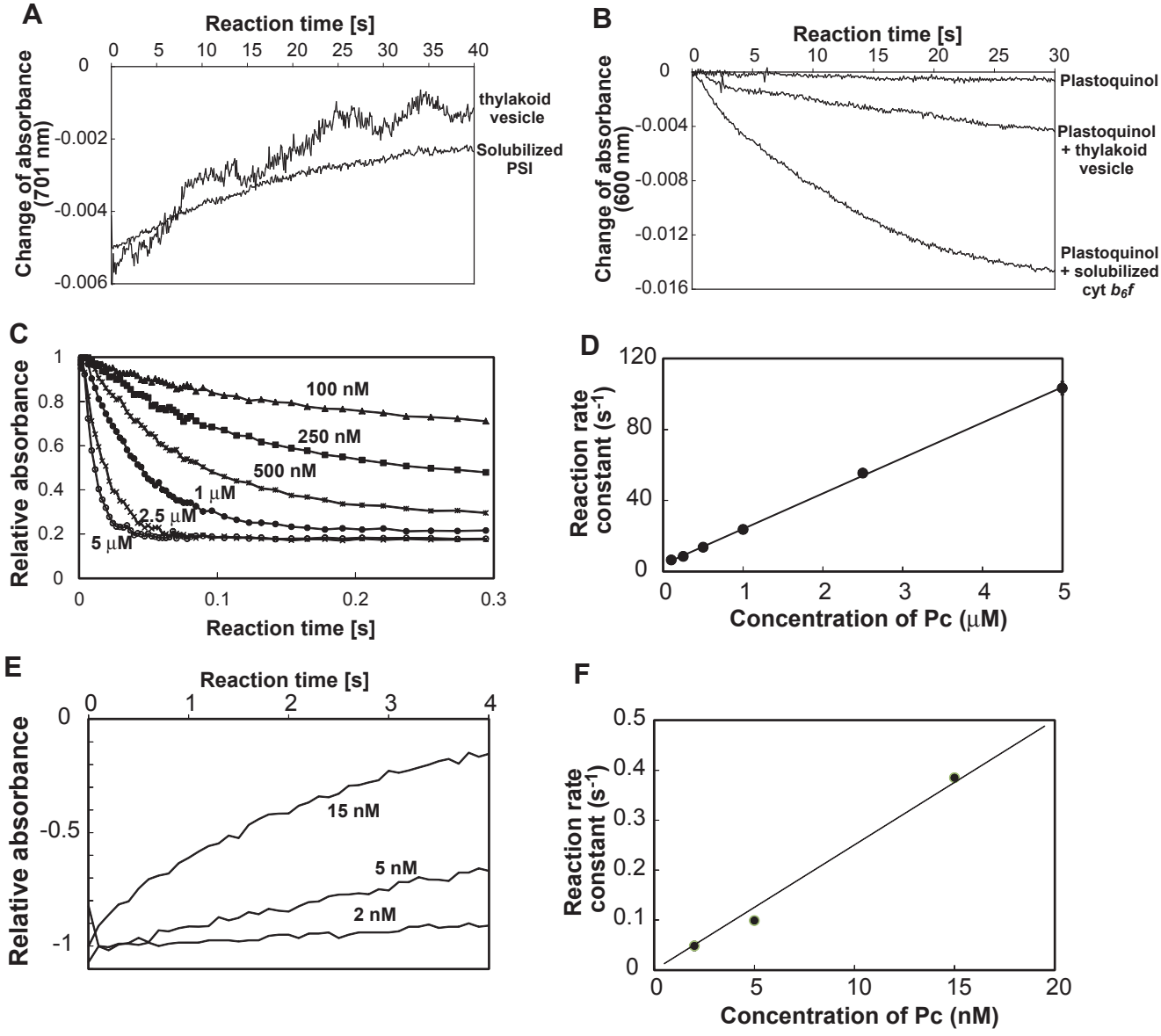

Supplementary Fig. 2 Electron transport activities of the obtained thylakoid vesicles and solubilized PSI and cyt *b*$_6$*f*.

A. Time course of the absorbance change at 701 nm of the solution containing 200 nM solubilized PSI or inside-out vesicles containing 200 nM PSI and 2 nM Pc, after the flash. The reduction of P700 by the Pc-PSI electron transport was monitored as the time-dependent recovery of the absorbance at 701 nm. The traces were averaged from four flash-photolysis experiments.

B. Time course of the absorbance change at 600 nm, after mixing 1 nM solubilized cyt *b*$_6$*f* or inside-out vesicles containing 2 nM cyt *b*$_6$*f* with 5 μM Pc and 15 μM decylplastoquinol. The oxidation of Pc by the Pc-cyt *b*$_6$*f* electron transport was monitored as the time-dependent decrease of the absorbance at 600 nm.

C-D. Stopped-flow analyses of the electron transport activity of Pc for the solubilized cyt *b*$_6$*f*. C. Time course of the change in the absorbance at 421.2 minus 410.5 nm, after mixing 0.15 μM reduced and solubilized cyt *b*$_6$*f* with various concentrations of the oxidized wild type Pc. The absorbances were devided by that immediately after the reaction. The traces were averaged from eight stopped-flow experiments. D. Plots of the reaction rate constants against the concentration of Pc. Error bars, which represent the standard errors of eight experiments, were within the range of the marker size.

E-F. Pc concentration dependence of the electron transport activity of Pc for the solubilized PSI. E. Time course of the change at 701 nm of the solution containing 200 nM solubilized and various concentrations of Pc, after the flash. The absorbances were divided by that immediately after the reaction. The traces were averaged from three to four experiments. F. Plots of the reaction rate constants against the concentration of Pc. Error bars, which represent the standard errors of four experiments, were within the range of the marker size.

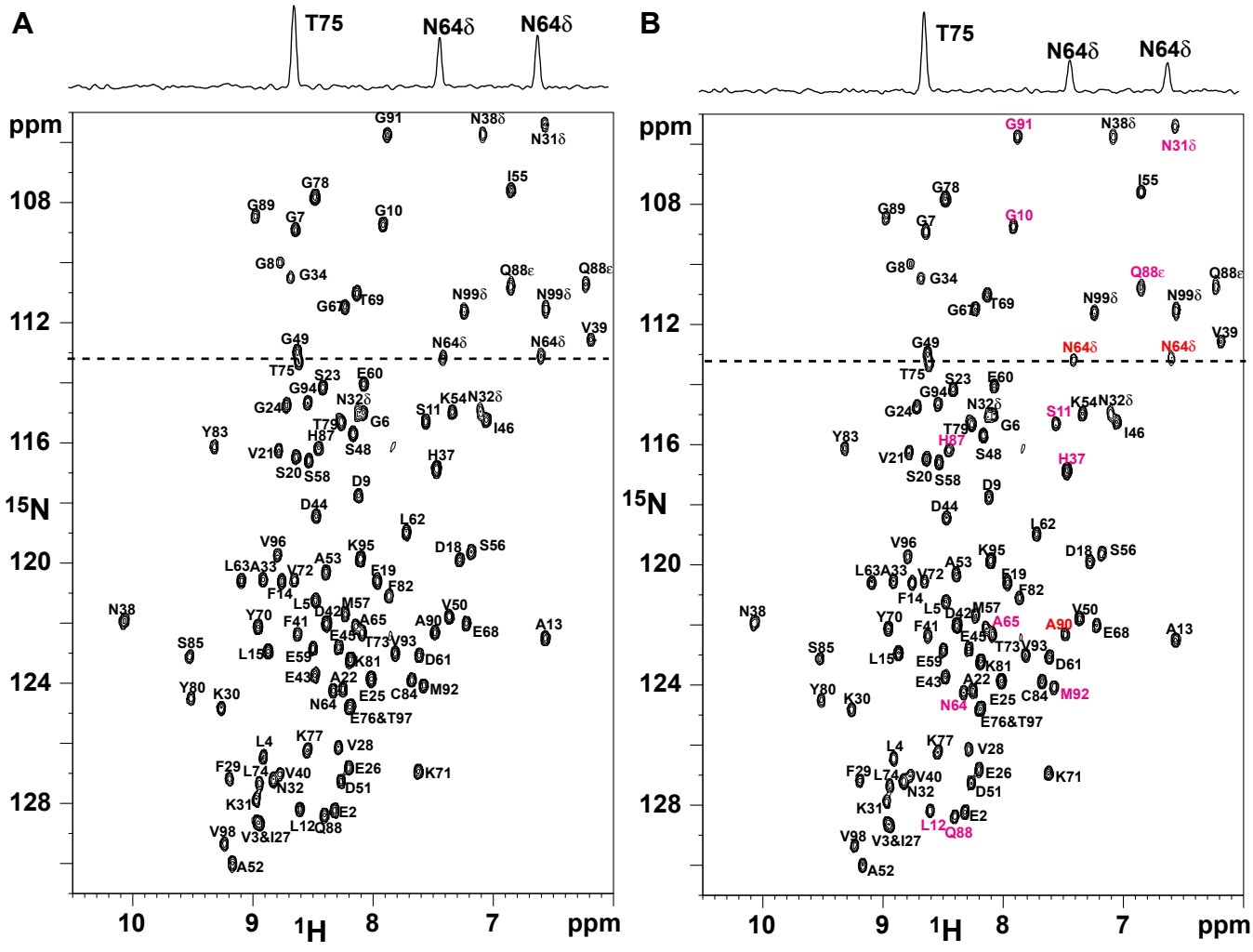

Supplementary Fig. 3 [^{1}H-^{15}N] shift correlation spectra observed at 18.8 T for excess amounts of uniformly [^{2}H,^{15}N]-labeled Pc relative to the PSI and cyt *b*$_6$*f* embedded in thylakoid vesicles, without (A) and with (B) irradiation.
One-dimensional cross-sections are also shown for the resonances from the Thr-75 and Asn-64 sidechains, where small but significant intensity reductions were observed. The residues with signal intensity reduction ratios > 0.3 and within the 0.2-0.3 range are colored red and pink, respectively. The resonances from Gly-17 (^{1}H: 7.89 ppm, ^{15}N: 101.0 ppm), Phe-35 (^{1}H: 5.62 ppm, ^{15}N: 114.8 ppm), the His-37 sidechain (^{1}H: 11.51 ppm, ^{15}N: 127.9 ppm) and Asn-99 (^{1}H: 8.87 ppm, ^{15}N: 132.8 ppm) are not displayed in

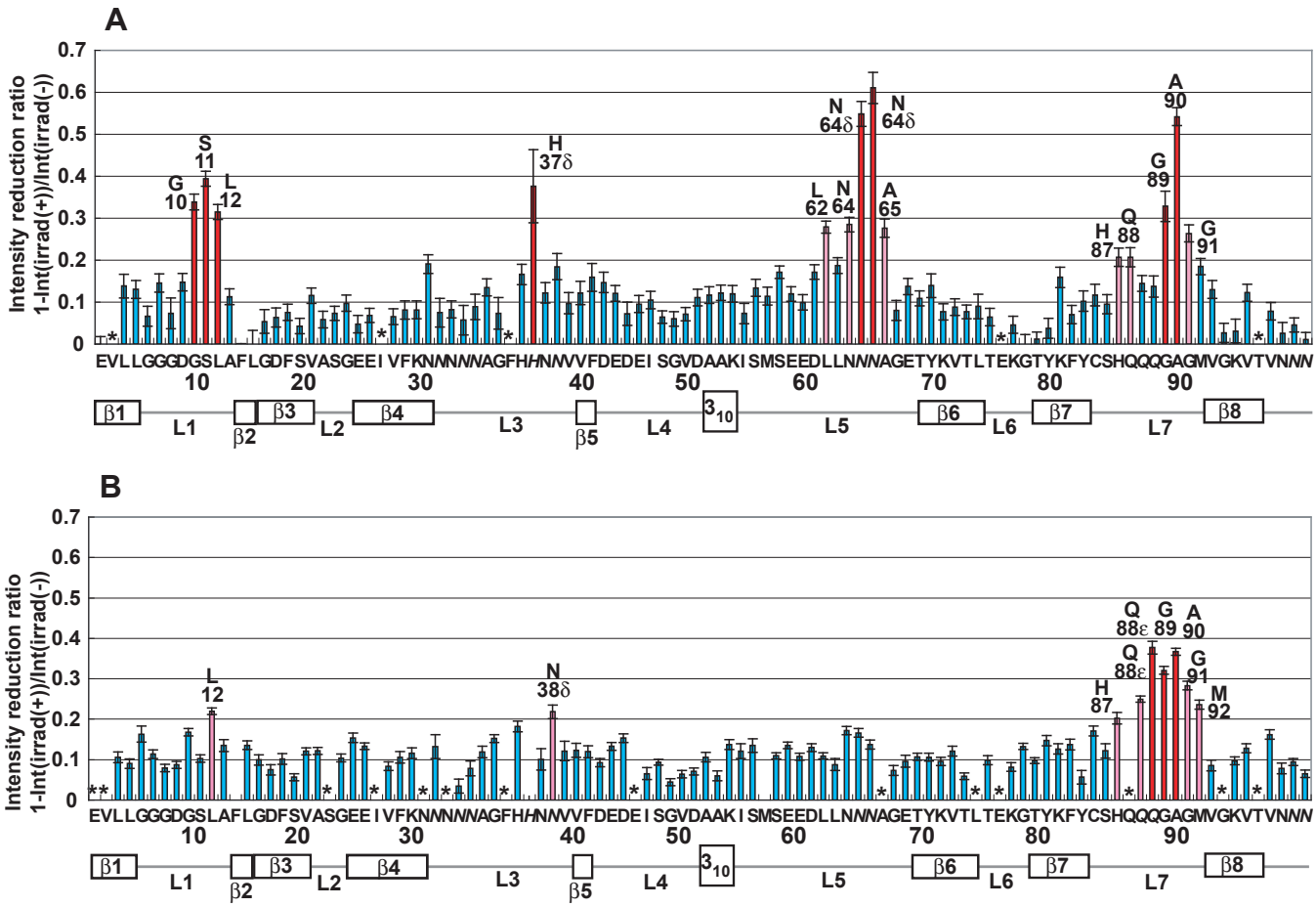

Supplementary Fig. 4 Plots of the reduction ratios of the signal intensities originating from the amide groups, with and without presaturation, in the TCS experiments with an excess amount of Pc relative to the solubilized (A) PSI or (B) cyt *b*$_6$*f*.

The labeling and coloring schemes are the same as in Fig.2B. The affected residues are mapped in Figs. 3B and 4B, respectively.

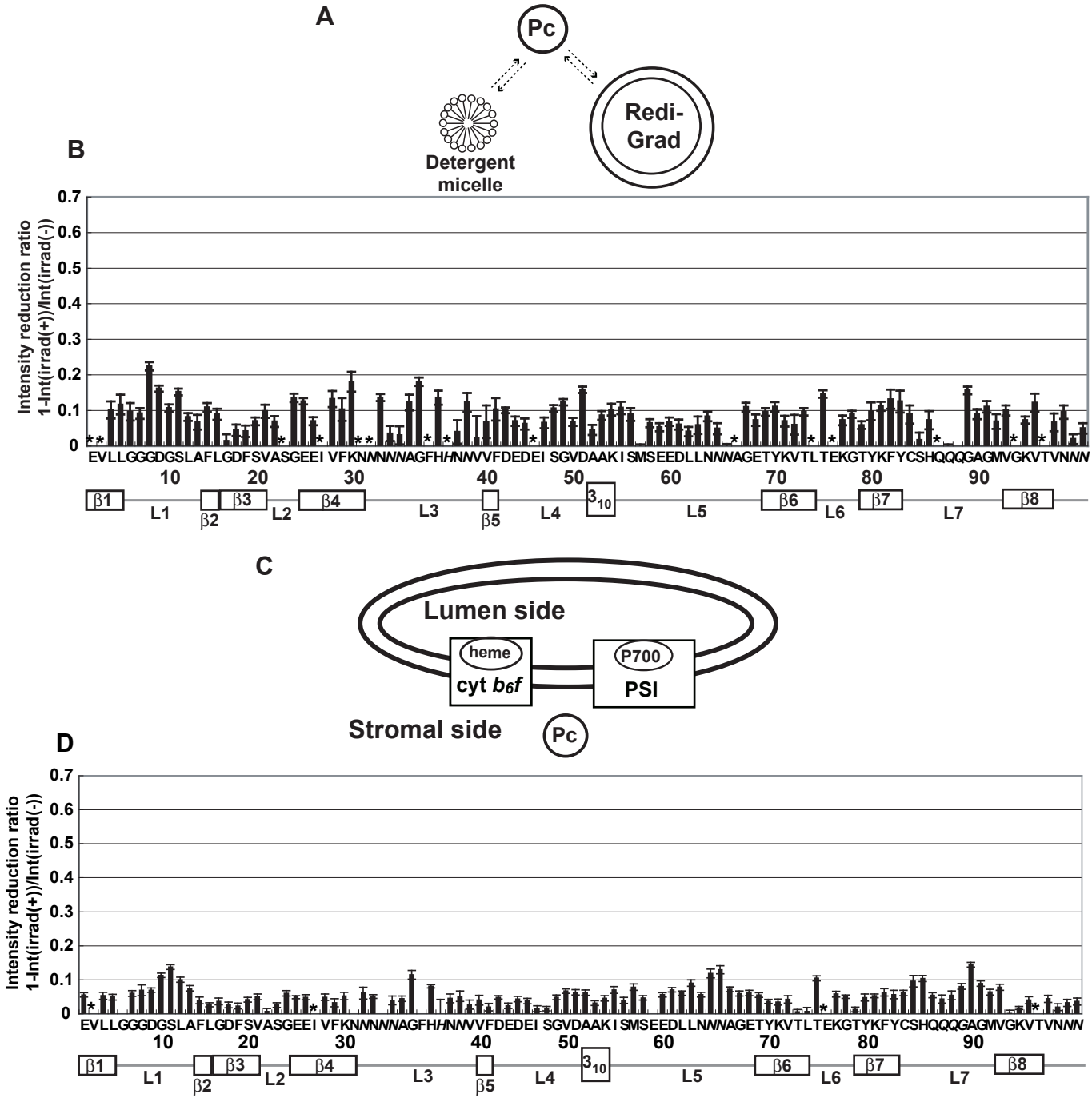

Supplementary Fig. 5 Investigation of the effects of residual protons and non-specific binding.

A-B. TCS experiments of Pc with additives.

A. Schematic diagram of the experiments.

B. Plots of the reduction ratios of the signal intensities originating from the amide groups, with and without presaturation, in the TCS experiments of Pc with additives. The primary sequence, the secondary structure, and the residue numbers of Pc are displayed in the single-letter amino acid code (sidechains are denoted in italic). The error bars represent the root sum square of the reciprocal of the signal-to-noise ratio of the resonances with and without irradiation. Asterisks represent the residues with intensity reduction ratios that were not determined, due to low signal intensity or spectral overlap.

C-D. TCS experiments of Pc with right side-out vesicles.

C. Schematic diagram of the experiments. In the right side-out vesicles, the Pc binding sites of PSI and cyt *b*$_6$*f* are inwardly directed.

D. Plots of the reduction ratios of the signal intensities originating from the amide groups, with and without presaturation.

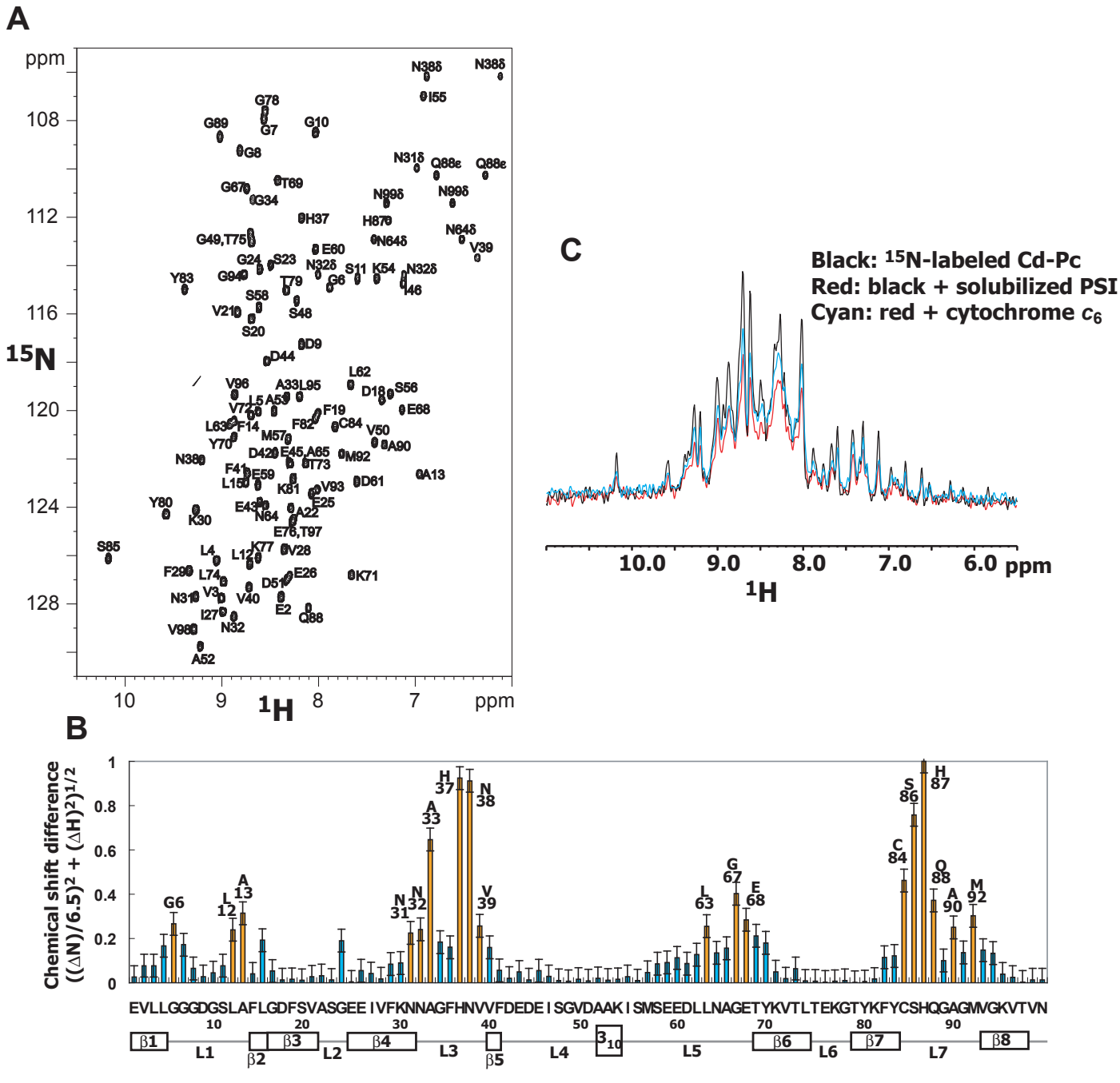

Supplementary Fig. 6 Characterization and TCS experiments of Cd-Pc. A. [^{1}H-^{15}N] shift correlation spectra observed at 9.4 T for uniformly [^{15}N]-labeled Cd-Pc dissolved in 10 mM NaPi, pH 6.0 and 10 % D_2O. The resonances from Gly-17 (^{1}H: 8.00 ppm, ^{15}N: 101.1 ppm), Phe-35 (^{1}H: 5.83 ppm, ^{15}N: 115.2 ppm), Gly-91 (^{1}H: 7.87 ppm, ^{15}N: 104.8 ppm) and Asn-99 (^{1}H: 8.92 ppm, ^{15}N: 132.7 ppm) are not displayed in these spectra. B. Plots of the chemical shift difference between Pc and Cd-Pc. The chemical shift difference values were normalized. Orange and cyan plots represent the residues with normalized chemical shift difference values > 0.2 and < 0.2, respectively. The primary sequence, secondary structure, and the residue numbers of Pc are displayed in single-letter amino acid code. The error bars were calculated based on the digital resolution. C. overlay of the 1D-projection of ^{1}H-^{15}N shift correlation spectra of ^{15}N-labeled Pc in free form (black), with solubilized PSI (red), and with cyt c_6 (blue).

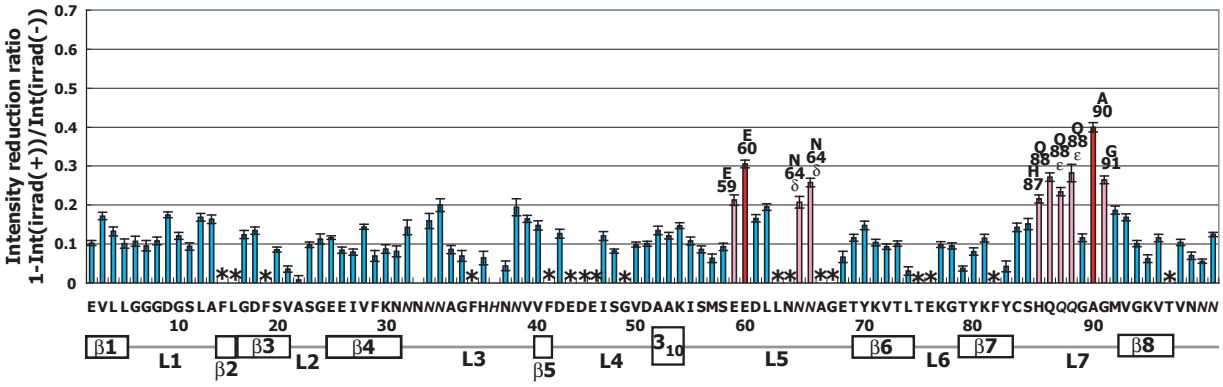

Supplementary Fig. 7 Plots of the reduction ratios of the signal intensities originating from the amide groups, with and without presaturation in the TCS experiments with excess amount of Cd-Pc relative to the solubilized PSI.
The labeling and coloring schemes are the same as in Fig.2B. The mappings of the affected residues are shown in Fig. 6B.

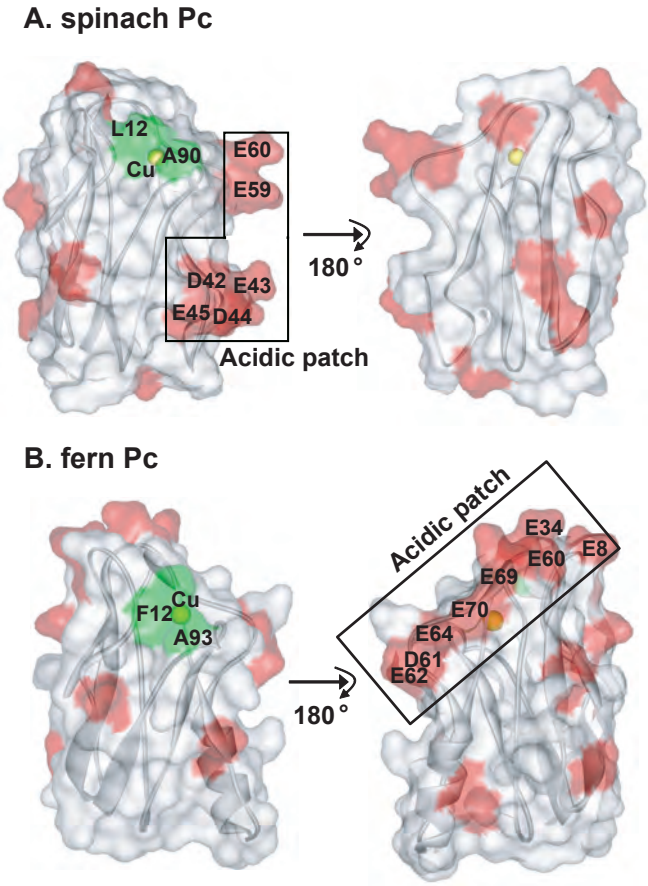

Supplementary Fig. 8 Distribution of the acidic residues in spinach (A) and fern (B) Pcs.
The acidic residues are colored red on the structures of spinach and fern Pcs. L12 and A90 in spinach Pc, and their corresponding residues in fern Pc (F12 and A93), are colored green. The regions where acidic residues are localized are labeled and enclosed with squares. The molecular diagrams were generated with Web Lab Viewer Pro (Molecular Simulations, Inc.).

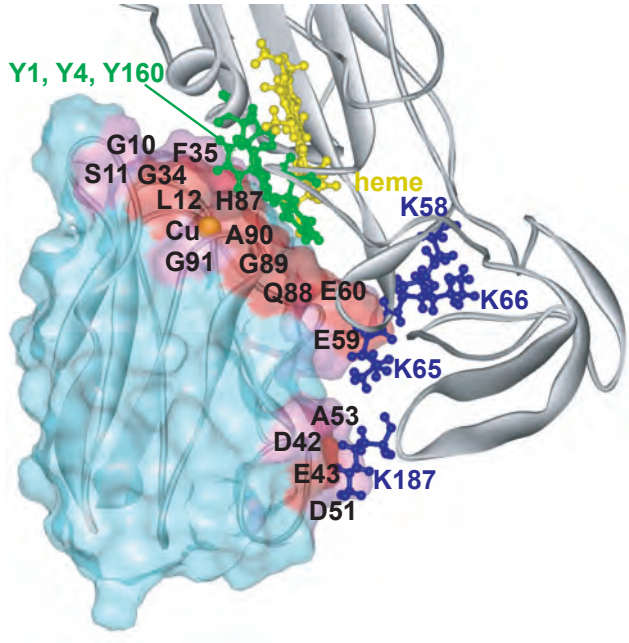

Supplementary Fig. 9 Mapping of the residues of Pc close to cyt *f* in the previously proposed structure of the electron transfer complex between Pc and cyt *f*.

The residues of Pc with Sum(r) < 3.5 Å and within the 3.5 - 4.5 Å range are labeled and colored red and pink, respectively, in the previously proposed structure of the spinach Pc-turnip cyt *f* complex (Ubbink et al., 1998) . Other Pc residues are cyan. The surface of Pc is transparent, and the copper atom and the ribbon diagram are simultaneously displayed. The hydrophobic and basic residues of cyt *f* that were proposed to be responsible for the electron transport by previous mutational studies (Soriano et al., 1996; Soriano et al., 1998; Gong et al., 2000a) are colored green and blue, respectively. The heme molecule is colored yellow.

	R_α (s^{-1})	R_β (s^{-1})	η_{xy} (s^{-1})	τ_{cobs} ($x10^{-9}$ s)	D_{dss} ($x10^{-6}$ cm^2 s^{-1})
0.1 mM uniformly [^{2}H,^{15}N]-labeled Pc (303K)	3.4	15.0	5.8	3.6	5.34
0.1 mM uniformly [^{2}H,^{15}N]-labeled Pc (283 K)	4.1	22.7	9.3	6.5	2.84
0.1 mM uniformly [^{2}H,^{15}N]-labeled Pc + 10 μM solubilized PSI (303K)	13.9	70.0	28.1	20.0	5.22
0.1 mM uniformly [^{2}H,^{15}N]-labeled Pc + 20 μM solubilized cyt b_6f (303K)	14.4	85.4	35.5	26.0	4.91

Supplemental Table 1 Amide ^{15}N transverse cross-correlated relaxation rate, η_{xy}, and apparent rotational correlation time, τ_{cobs}, of uniformly [^{2}H,^{15}N]-labeled Pc with substoichiometric amounts of PSI and cyt b_6f determined by TRACT experiments, and the diffusion coefficient of DSS in the sample, D_{dss}.

PDB entry	**Chain ID**	**Acidic residue**	**Partner**	**Sum(r) (Å)**
1UGH	I	D61	K218	4.5
1WMH	A	E65	K19	3.1
1WMH	A	E65	R89	3.1
1WMH	A	D67	K19	3.1
1XG2	B	D116	K224	3.8
1EUV	A	D451	R64	2.4
1EUV	B	D68	R489	3.3
1EUV	B	E94	R438	3.8
1F3V	B	D445	R146	4.5
1QAV	A	D143	R1019	2.4
1GAQ	B	D65	K91	2.8
1TKW	A	E43	R209	3.6
2PCF	A	E43	K187	2.8

Supplemental Table 2 Sum(r) of the salt bridges in various protein-protein complex structures.

Primer name	Sequence
(i) Primers for construction of spinach Pc gene	
Primer 1	GGAATTCCATATGCTACGTAAACTCGCTGCCGTATCCCTGCTGTCC CTGCTCAGTGCGCCGCTGTTGGCCGTTGAGGTGT
Primer 2	GAGGCTACGCTGAAGTCTCCTGGAAGGAATGCCAAAGAACCGTCA CGCCACCCGAGCAACACCTCAACGGCCAACAGCG
Primer 3	AGGAGACTTCAGCGTAGCCTCGGGCGAGGAGATCGTATTCAAGAA CAATGCCGGATTCCCCCACAACGTAGTGTTTGACG
Primer 4	TCCTCCTCGGACATCGAAATCTTCGCGGCGTCGACACCGGAGGGA ATCTCGTCCTCGTCAAACACTACGTTGTGGGGGAA
Primer 5	AAGATTTCGATGTCCGAGGAGGATTTGCTGAATGCACCAGGGGAA ACTTACAAAGTTACCCTTACTGAGAAAGGAACTTA
Primer 6	GTTACTTTTCCCACCATACCAGCACCCTGGTGGGGTGAGCAGTAG AACTTGTAAGTTCCTTTCTCAGTAAGGGTAACTTT
Primer 7	TGCTGGTATGGTGGGAAAAGTAACTGTCAACTAATGTACCCTGACC CTGAAGTGATGCGCGAGCGATCCGCTGCATGAAA
Primer 8	TTTTAAGCTTAGCCCGGCGCGCGCCCATGAAAAAGCCCGGCAGCG GCCGGGCTTTTTCATGCAGCGGATCGCTCG
(ii) Primers for construction of *Monoraphidium braunii* cytochrome c_6 gene	
Primer 1	GACGACGACAATCATATGGAGGCTGATCTGGCTCTGGGCAAAGC CGTGTTCGATGGCAAC
Primer 2	CGGAATCACGTTGTTCCCCCCGCCGGCGTGACACGCTGCACAG TTGCCATCGAACACGGC
Primer 3	GGGAACAACGTGATTCCGGATCACACCTTACAGAAGGCGGCAAT TGAGCAGTTTCTGGAC

Primer 4	CTCAATCTGATAGACAATGGCCTCAATATTAAAGCCTCCGTCCAGA AACTGCTCAATTGC
Primer 5	GCCATTGTCTATCAGATTGAGAACGGTAAAGGAGCCATGCCAGCC TGGGACGGCCGTCTG
Primer 6	ATCATATACATAGGCTGCTACACCCGCAATCTCATCTTCGTCCAGA CGGCCGTCCCAGGC
Primer 7	GCAGCCTATGTATATGATCAAGCGGCGGGCAATAAATGGTAAGTG TCCGGGCTTCTCC
Primer 8	GAGGAGAAGCCCGGACACTTACCA

Supplemental Table 3 Primers for the construction of spinach Pc and *Monoraphidium braunii* cytochrome c_6.

Supplemental Discussion

Analyses of the intensity reduction of the resonances from free Pc upon the addition of PSI and/or cyt b_6f

The intensity reduction of the resonances from Pc, upon the addition of a substoichiometric amount of PSI and/or cyt b_6f, suggests the increase of τ_c of the free Pc. The transverse cross-correlated relaxation rates of the amide nitrogen atoms (η_{xy}) of Pc with a substoichiometric amount of the solubilized PSI or cyt b_6f, which were determined by the 1D transverse relaxation-optimized spectroscopy for rotational correlation times (TRACT) experiments (Lee et al., 2006), were significantly larger than those for free Pc (Supplemental Table 1 online). The increase of η_{xy} suggests the increase of the averaged correlation time of the rotational Brownian motion (τ_{cobs}) (Supplemental Table 1 online). We confirmed that the increase of τ_{cobs} is not induced by the detergents. There are two possibilities for the increase of τ_{cobs} of the free Pc under the conditions with substoichiometric amounts of PSI and cyt b_6f : (i) interaction with huge PSI and cyt b_6f in the fast exchange mode, and (ii) increased viscosity of the sample. To examine the latter possibility, the viscosity of the sample was examined by determining the diffusion coefficients of 2,2-dimethyl-2-silapentane-5-sulfonate (DSS) in the samples (D_{DSS}), which were assessed by the pulsed field gradient (PFG) method (Nesmelova et al., 2004). As a result, the D_{DSS} values were not significantly decreased upon the addition of the solubilized PSI or cyt b_6f. On the other hand, a decrease of D_{DSS} was observed with an increase of the viscosity, generated by lowering the temperature from 303 K to 283 K (Supplemental Table 1 online), suggesting that the D_{DSS} was precisely determined. Therefore, the increase of the τ_{cobs} is due to the

interaction between Pc and the substoichiometric amount of huge PSI or cyt b_6f in the fast exchange mode.

At least in the interaction between cadmium-substituted Pc and PSI, the signal intensity was recovered by *Monoraphidium braunii* cytochrome c_6, which reportedly binds to the Pc-binding site of PSI and, like Pc, donates an electron to photo-excited PSI (Hervas et al., 1995), suggesting that the intensity reduction is due to the specific interaction (Supplemental Fig. 6 online, *vide infra)*, although we could not observe this effect for Pc-PSI complex, because the affinity of Pc for PSI is too high to observe this competitive effect.

Statistical analyses of salt bridge structures

To examine whether the salt bridges can be identified by the TCS experiment, we investigated the distance between the acidic residues that form intermolecular salt bridges and their binding partners in the protein-protein complex structures deposited in the Protein Data Bank (PDB). The distances are represented by *Sum*(r):

$$Sum(r) = \left(\sum_i r_i^{-6} \right)^{-\frac{1}{6}}$$

where r_i is the distance between an amide proton of each acidic residue and the ith proton of the binding partner. Thirteen intermolecular salt bridges were found in the nine structures, and all of the acidic residues that form intermolecular salt bridges have *Sum*(r) smaller than 4.5 Å (Supplemental Table 2 online). Our relaxation matrix

calculations revealed that the residues with *Sum*(r) less than 4.5 Å are affected by irradiation in the TCS experiments. Therefore, we concluded that the acidic patch residues of Pc do not form stable salt bridges with either PSI or cyt b_6f.

These conclusions are supported by the fact that the proportion of the acidic residues in the binding interfaces of protein-ligand complexes, determined from previously reported cross-saturation experiments, is 10 % (33 out of 337), which is almost identical to the proportion from X-ray structures (13 %) (Chen and Zhou, 2005). In addition, in the TCS experiments of the solubilized PSI and the cadmium-substituted Pc, Glu-59 and Glu-60 were significantly affected by irradiation (Fig. 6). These results further support the conclusions that we can detect the electrostatic interactions by TCS.

SUPPLIMENTAL REFERENCES

Chen, H., and Zhou, H.X. (2005). Prediction of interface residues in protein-protein complexes by a consensus neural network method: test against NMR data. Proteins **61,** 21-35.

Gong, X.S., Wen, J.Q., and Gray, J.C. (2000). The role of amino-acid residues in the hydrophobic patch surrounding the haem group of cytochrome *f* in the interaction with plastocyanin. Eur J Biochem **267,** 1732-1742.

Hervas, M., Navarro, J.A., Diaz, A., Bottin, H., and De la Rosa, M.A. (1995). Laser-flash kinetic analysis of the fast electron transfer from plastocyanin and cytochrome c_6 to photosystem I. Experimental evidence on the evolution of the reaction mechanism. Biochemistry **34,** 11321-11326.

Lee, D., Hilty, C., Wider, G., and Wüthrich, K. (2006). Effective rotational correlation times of proteins from NMR relaxation interference. J. Magn. Reson. **178,** 72-76.

Nesmelova, I.V., Idiyatullin, D., and Mayo, K.H. (2004). Measuring protein self-diffusion in protein-protein mixtures using a pulsed gradient spin-echo technique with WATERGATE and isotope filtering. J. Magn. Reson. **166,** 129-133.

Soriano, G.M., Ponamarev, M.V., Tae, G.S., and Cramer, W.A. (1996). Effect of the interdomain basic region of cytochrome f on its redox reactions in vivo. Biochemistry **35,** 14590-14598.

Soriano, G.M., Ponamarev, M.V., Piskorowski, R.A., and Cramer, W.A. (1998). Identification of the basic residues of cytochrome f responsible for electrostatic docking interactions with plastocyanin in vitro: relevance to the electron transfer reaction in vivo. Biochemistry **37,** 15120-15128.

Ubbink, M., Ejdeback, M., Karlsson, B.G., and Bendall, D.S. (1998). The structure of the complex of plastocyanin and cytochrome *f* , determined by paramagnetic NMR and restrained rigid-body molecular dynamics. Structure **6,** 323-335.